

Water Resources Research

RESEARCH ARTICLE

10.1029/2019WR025116

Key Points:

- Two regimes of particle motions are identified for long- and short-distance hops
- Long-distance hops lead to Gaussian-like velocity distribution and exponential-like tail of hop distance distribution
- Short-distance hops give rise to the Weibull-like front of hop distance distribution

Correspondence to:

Z. Wu and E. Fofoula-Georgiou,
wuzi@pku.edu.cn;
efi@uci.edu

Citation:

Wu, Z., Furbish, D., & Fofoula-Georgiou, E. (2020). Generalization of hop distance-time scaling and particle velocity distributions via a two-regime formalism of bedload particle motions. *Water Resources Research*, 56, e2019WR025116. <https://doi.org/10.1029/2019WR025116>

Received 7 MAR 2019

Accepted 21 OCT 2019

Accepted article online 6 NOV 2019

Generalization of Hop Distance-Time Scaling and Particle Velocity Distributions via a Two-Regime Formalism of Bedload Particle Motions

Zi Wu^{1,2} , David Furbish^{3,4} , and Efi Fofoula-Georgiou^{2,5} 

¹State Key Laboratory of Hydrosience and Engineering, Department of Hydraulic Engineering, Tsinghua University, Beijing, China, ²Department of Civil and Environmental Engineering, University of California, Irvine, CA, USA, ³Department of Earth and Environmental Sciences, Vanderbilt University, Nashville, TN, USA, ⁴Department of Civil and Environmental Engineering, Vanderbilt University, Nashville, TN, USA, ⁵Department of Earth System Science, University of California, Irvine, CA, USA

Abstract To date, there is no consensus on the probability distribution of particle velocities during bedload transport, with some studies suggesting an exponential-like distribution while others a Gaussian-like distribution. Yet, the form of this distribution is key for the determination of sediment flux and the dispersion characteristics of tracers in rivers. Combining theoretical analysis of the Fokker-Planck equation for particle motions, numerical simulations of the corresponding Langevin equation, and measurements of motion in high-speed imagery from particle-tracking experiments, we examine the statistics of bedload particle trajectories, revealing a two-regime distance-time ($L-T_p$) scaling for the particle hops (measured from start to stop). We show that particles of short hop distances scale as $L \sim T_p^2$ giving rise to the Weibull-like front of the hop distance distribution, while particles of long hop distances transition to a different scaling regime of $L \sim T_p$ leading to the exponential-like tail of the hop distance distribution. By demonstrating that the predominance of mostly long hop particles results in a Gaussian-like velocity distribution, while a mixture of both short and long hop distance particles leads to an exponential-like velocity distribution, we argue that the form of the probability distribution of particle velocities can depend on the physical environment within which particle transport occurs, explaining and unifying disparate views on particle velocity statistics reported in the literature.

Plain Language Summary The complex motion of sediment particles on a riverbed dictates the rate of bedload sediment transport with important implications for water quality, biotic life, and infrastructure safety. Inferring characteristics of individual particle trajectories from collective statistics of particle motion attributes (velocities, accelerations, hop distances, and travel times) is a challenge with significant theoretical and practical implications, including probabilistic formulations of transport, correct interpretation of experimental measurements, and comparison of disparate environmental transport conditions in rivers. Here, we document and physically explain two distinct regimes of particle motion, namely that short and long hop distance particles exhibit different dynamics, particle statistics, and hop distance-travel time scaling regimes. This finding explains and unifies disparate views on particle velocity statistics reported in the literature, provides the basis for interpreting experimentally constrained results, and clarifies the tail characteristics of particle hop distances, which is important for understanding anomalous bedload diffusion.

1. Introduction

Bedload sediment transport and the complex bedforms formed on the riverbed exert significant control on aquatic life, water quality, and infrastructure safety (Dingle et al., 2017; Hoefel & Elgar, 2003; Wilcock, 1998). Sediment particles transported as bedload within a turbulent flow undergo complex motions in response to forces exerted on them by near-bed turbulence, particle-particle interactions, and particle-bed interactions. Particle motions involve rolling, sliding, and low saltations, and individual particle hop distances—measured from start to stop—can be very small (displacements of only a few particle diameters) to very large (involving tens of collisions with the bed between the onset and cessation of motion) (Fathel et al., 2015; Furbish et al., 2016; Hosseini-Sadabadi et al., 2019; Nikora et al., 2002). Although the complex motion of bedload particles has been a centerpiece of a century of study of sediment transport, it is only

recently that innovative high-speed imaging measurement techniques (Fathel et al., 2015; Houssais et al., 2015; Lajeunesse et al., 2010; Roseberry et al., 2012; Yager et al., 2015) and advanced numerics for coupled fluid-particle motions (Fan et al., 2016; Kidanemariam & Uhlmann, 2014; Schmeeckle, 2014) have allowed a clear description of individual and collective particle motions, promising deeper understanding of their physics.

When viewed at timescales longer than those associated with the ballistic-like behavior of particles between successive particle-bed collisions (Furbish, Roseberry, & Schmeeckle, 2012; Nikora et al., 2002), bedload particle motions are inherently stochastic. Thus, probabilistic descriptions of particle motions and transport, building from the pioneering work of Einstein (Einstein, 1937; Einstein, 1950), have been the topic of intense research over the past decade (Ancey & Heyman, 2014; Furbish, Haff, et al., 2012; Furbish, Roseberry, & Schmeeckle, 2012; Ganti et al., 2010; Hassan et al., 2013; Hill et al., 2010; Martin et al., 2012; Nikora et al., 2002; Parker et al., 2000; Schumer et al., 2009; Voller & Paola, 2010; Wu, Foufoula-Georgiou, et al., 2019; Wu, Singh, et al., 2019). Three variables are of particular interest in describing the stochastic transport of bedload particles: particle velocities (and associated particle accelerations), particle hop distances (and associated particle travel times), and particle rest times between hops. To date, there is no consensus on disparate views of the probability distribution of particle velocities, except that the specific form of the distribution may be related to flow and transport intensities. That is, while some studies suggest an exponential-like distribution (Furbish et al., 2016; Furbish & Schmeeckle, 2013; Lajeunesse et al., 2010; Roseberry et al., 2012) for subcritical flows, others show a Gaussian-like distribution (Ancey & Heyman, 2014; Martin et al., 2012) under supercritical flow conditions. Together with the particle activity, the mean particle velocity determines the advective part of the sediment flux (Bridge & Dominic, 1984; Furbish, Haff, et al., 2012; Lajeunesse et al., 2010; Parker et al., 2003; Wong et al., 2007), and the variance of the velocities determines the diffusive part (Ancey & Heyman, 2014; Furbish, Haff, et al., 2012; Furbish, Roseberry, & Schmeeckle, 2012), so understanding and reaching consensus on the reasons for the reported discrepancies are fundamental for further progress.

In addition to bedload particle velocities, particle hop distances play an important role in probabilistic sediment transport formulations, for example, the entrainment form of the Exner equation for bedload sediment transport. In particular, the statistical behavior of large hop distances (i.e., the tail of the distribution) determines the type of diffusion, for example, normal (when the tail is exponential like) or superdiffusion (when the tail is power law type) with implications for the characteristic scale of spreading of sediment and pollutants attached to sediment particles. For example, in the absence of particle burial and exhumation, the hop distances dominate the spreading behavior, possibly including superdiffusion (Ganti et al., 2010; Schumer et al., 2009). In the presence of burial, the hop distances are responsible for determining where the particles are delivered and consequently their likelihood of burial (Iwasaki et al., 2017; Wu, Foufoula-Georgiou, et al., 2019; Wu, Singh, et al., 2019). Both cases bear on predicting not only bedload sediment transport but also the arrival of pollutants at locations downstream of a contaminant release with consequences for water quality and aquatic life.

Here we revisit the problem of the distribution of particle velocities in conjunction with the joint distribution of hop distances (L) and travel times (T_p). We start from the theoretical analysis in section 2 regarding the Fokker-Planck equation governing the bedload particle velocity variations, during which the two key functions of drift and diffusion are determined based on experimental data and the equilibrium transport conditions. The resulting governing equation is then applied in a Monte Carlo particle-tracking simulation. In section 3 we argue for a transition in scaling for particle hops based on experimental data and the high-fidelity simulation results, revealing that particles with short hop distances scale as $L \sim T_p^2$ and long hop distances as $L \sim T_p$. Then we show distinct motion characteristics between short and long hops, as well as how these distinctions can lead to different statistics for bedload particle motions including velocity and hop distance distributions. Discussion and concluding remarks are provided in the last two sections, respectively.

2. Formulation

2.1. The Governing Fokker-Planck Equation

For the purpose of simplification while still not compromising the underlying physical insights, we focus on the idealized case of uniform size bedload particles being transported under equilibrium conditions, and all discussions are restricted to the one-dimensional (streamwise) problem. The numerical simulation used in

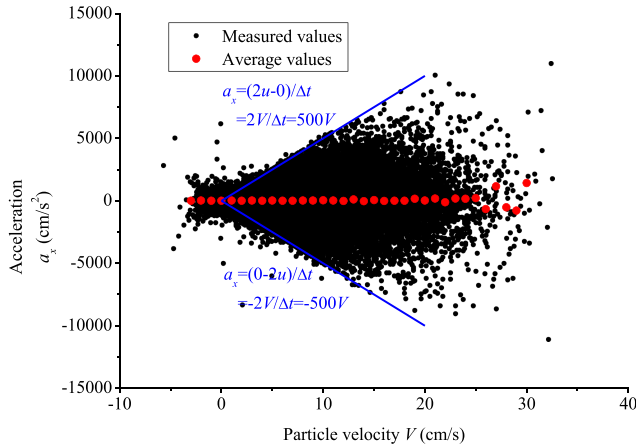


Figure 1. Particle acceleration versus particle velocity. Measured values and average values for 1 cm/s velocity increments are illustrated. The particle velocity is defined as $V = [u(t + \Delta t) + u(t)]/2$ and the particle acceleration as $a_x = [u(t + \Delta t) - u(t)]/\Delta t$, where $u(t)$ is the instantaneous velocity at time t . The data are from Run 1 reported in reference (Fathel et al., 2015). The results show that for any given velocity, the average acceleration is zero, indicating $\mu(u) = \mu = 0$.

this paper is based on the theoretical analysis of the Fokker-Planck equation. In statistical mechanics, the Fokker-Planck equation is a partial differential equation describing the time evolution of the probability density function (PDF) of a particle's velocity under different forces:

$$\frac{\partial P(u, t)}{\partial t} = -\frac{\partial}{\partial u} [\mu(u) P] + \frac{\partial^2}{\partial u^2} [k(u) P], \quad (1)$$

which has recently been shown to be able to describe the transport process of bedload particles (Furbish, Roseberry, & Schmeeckle, 2012). In the above equation, P is the velocity PDF, t is the time (s), μ (m/s²), and k (m²/s³) are respectively the “drift” and “diffusivity” with respect to the streamwise particle velocity u (m/s).

2.2. Determine the “Drift” μ by Experimental Data

A major challenge in applying equation (1) for studying bedload particle motions resides in the determination of the forms of the functions of $\mu(u)$ and $k(u)$. We note that the “drift” $\mu(u)$ (also known as “drift velocity” in statistical mechanics) in equation (1) does not represent an actual bedload particle velocity, but rather, it is a term borrowed from other fields in the study of the Fokker-Planck equation. Its physical meaning can be derived from its definition (Furbish, Roseberry, & Schmeeckle, 2012), which we rewrite in the following form under the equilibrium transport conditions

$$\mu(u) = \lim_{t \rightarrow 0} \frac{1}{dt} \int_{-\infty}^{+\infty} \Delta u f_{\Delta u}(\Delta u; u) d\Delta u. \quad (2)$$

In equation (2), Δu is the particle velocity change during a small time interval of dt , and $f_{\Delta u}$ is the probability density of a velocity change at a given velocity. Basically, the term

$$\int_{-\infty}^{+\infty} \Delta u f_{\Delta u}(\Delta u; u) d\Delta u$$

gives the mean velocity change at a given velocity; thus, equation (2) defines the “drift” $\mu(u)$ as the mean acceleration conditional on a given velocity.

So far there is no theory that tells us the form of $\mu(u)$. We only know that globally (over all u), the mean acceleration is zero for the equilibrium transport condition; otherwise, the particles (collectively) would be accelerating or decelerating. To empirically obtain information for $\mu(u)$ under equilibrium transport conditions, we plot the experimentally measured data (Fathel et al., 2015) in Figure 1. Specifically, we calculate the acceleration $a_x = [u(t + \Delta t) - u(t)]/\Delta t$, which is associated with the velocity of $V = [u(t + \Delta t) + u(t)]/2$, where $u(t)$ is the instantaneous velocity at time t . That is, the average velocity, or the linear interpolation for an intermediate velocity, is considered during the velocity variation. The vertical symmetry of data points in Figure 1 implies an equal chance of accelerating and decelerating of particles associated with any pair of successive velocities u_1 and u_2 . We note that accelerations can be much greater than those illustrated in Figure 1 when resolved at smaller time stepping. We clarify that the adopted experimental time step of $\Delta t = 0.004$ s in this paper cannot resolve these higher magnitude accelerations, but effectively serves as a low-pass filter to smooth over them. It is possible that accelerations may be asymmetrical if measured at higher resolutions; however, the smoothing with the time step of 0.004 s reveals symmetry. By calculating mean accelerations for increments of the velocity values (i.e., equation (2) for $\mu(u)$; the red dots in Figure 1), we have the empirical result of $\mu(u) = \mu = 0$. This result indicates zero external forces exerted on particles with the same velocity V , serving as an additional constraint other than zero external forces on all particles as required by the equilibrium transport conditions. This finding revises and corrects previous assessments in the literature (Furbish, Roseberry, & Schmeeckle, 2012). For a given velocity V in Figure 1, the maximum measured

acceleration (in absolute value) is associated with a variation of instantaneous velocities between 0 and $2u$ (neglect the negative velocities), which is $\pm 2u/\Delta t$ and illustrated in Figure 1 by the envelope of $a_x = \pm 2u/\Delta t = \pm 2V/\Delta t = \pm 500V$, corresponding to the increasing width of the acceleration dispersion with increasing velocity. Thus, the highest positive acceleration (for a given velocity V) comes from an increase of velocity starting from 0, agreeing with that observed at the “entrainment phase” of particle motions as indicated by Campagnol et al. (2015). Note that a negative acceleration a_x for a given velocity V does not necessarily imply backward motions of the bedload particle (i.e., $u < 0$).

Based on this key result of $\mu(u) = \mu = 0$, equation (1) becomes

$$\frac{\partial P(u, t)}{\partial t} = \frac{\partial^2}{\partial u^2} [k(u) P]. \quad (3)$$

The equilibrium transport condition can be applied to determine $k(u)$ according to equation (3), which suggests that (1) $\frac{\partial P}{\partial t} = 0$ and (2) the probability flux should be zero across any velocity state (Lançon et al., 2001). The first requirement results in

$$\frac{\partial}{\partial u} [k(u) P(u)] = C \quad (4)$$

where C is a constant, while the second requirement indicates $C = 0$, leading to

$$k(u) \propto \frac{1}{P(u)}. \quad (5)$$

According to the experimental data (Fathel et al., 2015), we adopt $P(u) = f(u)$, where the exponential function

$$f(u) = \frac{1}{u_0} \exp\left(-\frac{u}{u_0}\right) \quad (6)$$

is an approximation of the exponential-like particle velocity PDF (Fathel et al., 2015), and $u_0 = 4.76$ cm/s is the mean velocity provided by the experimental results. Thus, we have

$$k(u) = c \exp\left(\frac{u}{u_0}\right), \quad (7)$$

where the constant c has the same dimension as k ($c = 300 \text{ m}^2/\text{s}^3$), which can be fitted to ensure preservation of the measured mean of absolute values of accelerations. We note that equation (7) does not imply an unbounded increase, but rather is a reasonable approximation as applied within the limited domain of measured/simulated velocities, which is consistent with equation (4). According to the above analysis, particle velocities and accelerations satisfying mechanical constraints of equilibrium transport conditions are embodied in the Fokker-Planck equation.

2.3. The Particle-Tracking Simulation

To develop and validate a model for simulating particle trajectories, we capitalize on a unique data set of particle motions collected by tracking bedload particles in 5 s of high-speed imagery (with a rate of 250 frames per second or sampling interval of 0.004 s), providing information on approximately 4,000 complete particle hops. See Figure 2 and references (Fathel et al., 2015; Furbish et al., 2016) for details.

In the experiment we have focused on independent particle hops, that is, a particle starts its motion, until again it ceases its motion; when and where a hop occurs is not considered in our analysis. To better track particles in experiments, an acrylic “sled” window is placed on the surface of the water to prevent light refraction, which may cause a particle to appear moving in the camera when in fact it is not. A particle is considered at rest if it does not move between successive frames. Particles that jiggle in

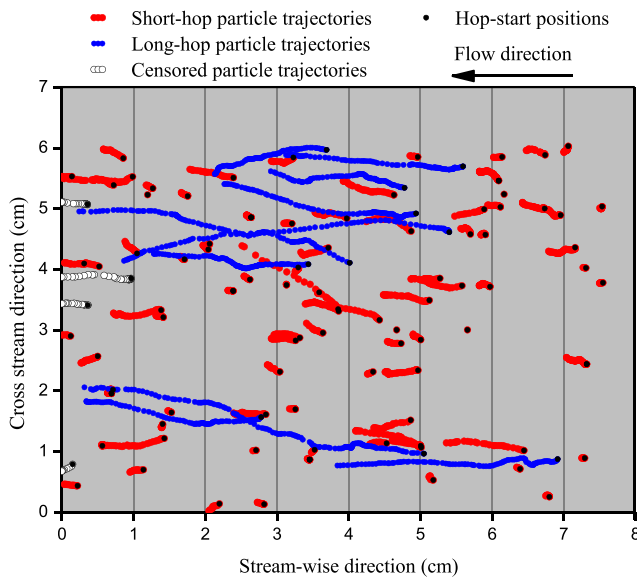


Figure 2. Illustration of observed particle trajectories. Ten trajectories for long hops, 96 for short hops, and 4 for censored hops were randomly selected from the experimental data set (Fathel et al., 2015) recorded at sampling interval of 0.004 s (250 frames per second) demonstrating that particle hop distances can vary from very small to large and that some of the particle hops are unavoidably censored due to experimental constraints. The criteria for distinguishing between short- and long-hop particles are discussed later in this paper. Focused on particle motions close to the left boundary of the observation area, both long- and short-hop particles are subject to the censorship effect in experiments, which means that particles may still be in motion while exiting the observational window. For this specific run of the experiment (Run 3 reported by Roseberry et al., 2012), the time-averaged velocity near the bed was 31 cm/s with a flow depth of 12.5 cm. The particles used in the experiment were uniform coarse sand with a mean diameter of 0.05 cm. For more details of this experiment as well as related theoretical considerations, please see also Furbish et al. (2016) and Fathel et al. (2015).

their pockets (i.e., when there is no net measurable displacement between its starting and ending positions during successive motions of a particle) are not tracked in the experiments, unless they are displaced from the pockets (Fathel et al., 2015). To compare with experimental results, in the particle-tracking simulation we focus on the same process: In each simulation we follow one particle when its motion starts, record its streamwise displacement after each time step (used to calculate instantaneous velocities and accelerations), and finish the simulation when the particle stops. We note that we are only interested in particle hops traveling in the positive flow direction, which dominate the bedload transport as revealed by experiments. Thus, we assume no negative velocity for numerical simulations (as indicated by equations (6) and (7)) and select forward hops in experiments for comparison.

We run the simulation 50,000 times (each for a hop of a single particle) to obtain a data set of 50,000 such hops. We note that for each particle hop, we collect the hop distance L , travel time T_p , and a series of velocity records during the entire hop. The 50,000 such series of velocity records are pooled together for analysis, that is, obtaining the velocity PDF, etc. Specifically, for the Monte Carlo simulation of the particle motions within each hop, we have the following discrete Lagrangian analogue to equation (3) (Dimou, 1989)

$$\Delta u = R\sqrt{2k(u)\Delta t}, \quad (8)$$

where R is a normally distributed random variable with zero mean and unit variance. It should be noted that although we do not explicitly specify what determines a bedload particle's movement under the equilibrium transport conditions (as a result of the combined actions of turbulent flow drag, particle-particle, and particle-bed interactions), we know statistically how the particle responds to these forces according to equation (8), that is, how its velocity should change with time, which provides key information for tracking the particle in the numerical simulation.

The time step is adopted as $\Delta t = 0.0004$ s; however, we resample the simulated results at a coarser time step of 0.004 s, which is the interval used in the experiments. In effect, this choice of resampling smooths the results, similar to what occurs with the experimental sampling interval, thus making the comparison between simulations and experiments more meaningful. Nonflux boundary conditions are applied for the numerical simulations, which indicates that during the particle motion, the particle velocity is bounded between the lower limit of zero (we neglect the negative velocity; Fathel et al., 2015) and the upper limit of u_{\max} . We note that u_{\max} is in accordance with the near-bed velocity of the fluid flow driving the particles, representing a physical constraint on the maximum particle velocity (Ancy & Heyman, 2014; Furbish & Schmeeckle, 2013). And it should also be noted that the exponential function equation (6) (determining the form of the diffusivity $k(u)$ in equation (7)) is only an approximation of the measured particle velocity PDF (Fathel et al., 2015), which in fact we term as “exponential like”. The maximum velocity is chosen as $u_{\max} = 30$ cm/s in the simulations according to the experimental measurements and because near-bed velocities limit the maximum velocities as elaborated in Roseberry et al. (2012) and Fathel et al. (2015), but the results are not sensitive to this value.

Based on the simulated results of equation (8), we have information about the velocity variations of a bedload particle, and its streamwise movement can be obtained by

$$\Delta x = u(t)\Delta t. \quad (9)$$

For simulating the hop events of bedload particles, we need to specify the initial condition

$$P(u, t)|_{t=0} = \delta(u), \quad (10)$$

indicating that all the particles start their motions from the velocity of $u = 0$. We then track each particle's movement according to equations (8) and (9). Each time when the particle velocity drops to (or below) zero, a particle has a chance of $s = 90\%$ to continue its motion (or the particle will stop, and the hop is finished), which is adopted so that the simulated mean travel time matches the observed mean. Equation (10) and the parameter $(1 - s)$ provide the starting and termination conditions for a specific particle hop, respectively.

The definition of constant stopping chance $(1-s)$ in the simulation is consistent with the constant disentrainment rate (failure rate) formulation of travel times, where stopping is a memoryless process. This means that if a particle is about to "hit zero velocity" and needs to "decide" whether or not to stop, its previous history is irrelevant (i.e., in the event of "hitting zero," all particles have the same chance to stop motion). On the other hand, the chance for a slow traveling (at time t) particle to "hit zero velocity" (at time $t + \Delta t$) is greater than that for a fast moving particle (e.g., the fast moving particle needs to decelerate first before "hitting zero velocity"). Based on the above arguments, it is evident that a particle performs long hops not because it hits zero many more times (than short hops) and survives, but because it spends more time traveling with velocities far from zero and does not need to hit zero many times. In other words, on the average, particles traveling with low velocities may perform a lot of "zero hits" and stop early (i.e., short-hop particles); only those particles that do not frequently hit zero velocity survive and turn out to be long-hop particles. At the same time, we are unable to identify the "zero hit" events by observing the velocity variations. Due to the nonflux boundary conditions in the simulation, when the particle is about to change its velocity from $u_1 > 0$ to $u_2 < 0$ (i.e., a "zero hit") due to the calculated velocity change, it will acquire a new velocity of $u = -u_2 (>0)$ if its motion is going to continue as decided by s . Thus, if we only look at the velocity records, there is no sign for this "zero hit" event, which is the same as observing a particle traveling slowly in the experiment. Physically, s may be related to the specific transport environment including the roughness of the bed, the flow strength, the particle diameter, etc., which determines how easily a particle can cease its motion.

According to the above documented numerical algorithm, only three parameters need to be calibrated during the numerical simulation of the particle hop. The constant velocity u_0 is the mean velocity of particles, the constant c in the "diffusivity" $k(u)$ generally determines how fast a particle can change its velocity, and the constant chance s generally determines how easily a particle can cease its motion. We note that no additional information regarding a particle's hop is prescribed, that is, whether it should be "short" or "long" in hop distance. Hence, nothing about the distance-time scaling of a particle hop is specified in the numerical model but rather both the scaling regimes and the regime transition emerge as a result of the prescribed particle motions.

3. Results

3.1. High-Fidelity Numerical Simulations

For the experimentally measured 4,000 particle hops, the probability distributions of velocities, accelerations, hop distances, and travel times are shown in Figure 3 (red dots). The particle velocity distribution has been previously referred to as "exponential like" and the acceleration distribution as "Laplace like" due to slight deviation from the exponential and Laplace form, respectively, in the tail of the PDF (Fathel et al., 2015; Roseberry et al., 2012). This deviation is clearly observed in the exceedance probability plots (Figures 3a and 3b inserts; compare the red dots with the exponential line). Particle velocities and accelerations satisfying constraints of equilibrium transport conditions are embodied in the Fokker-Planck equation which provides the theoretical basis for the developed numerical simulation scheme of particle trajectories (see section 2.3 for details). More specifically, the mean velocity and the mean of absolute values of accelerations in the experimental measurements can be used to determine the two constants of u_0 and c for the governing Fokker-Planck equation, respectively (i.e., see equation (7)).

A total of 50,000 particle trajectories were followed during our Monte Carlo simulation of particle hops, an order of magnitude larger than the size of the experimental data set. The simulation results confirm that, in agreement with the observations, the acceleration PDF is Laplace-like (Fathel et al., 2015; Furbish et al., 2016) (Figure 3b). The small misfit of accelerations (Figure 3b insert) is in part likely due to the spatial resolution of particle motion measurement, which is about 0.05 mm, resulting in a velocity resolution of

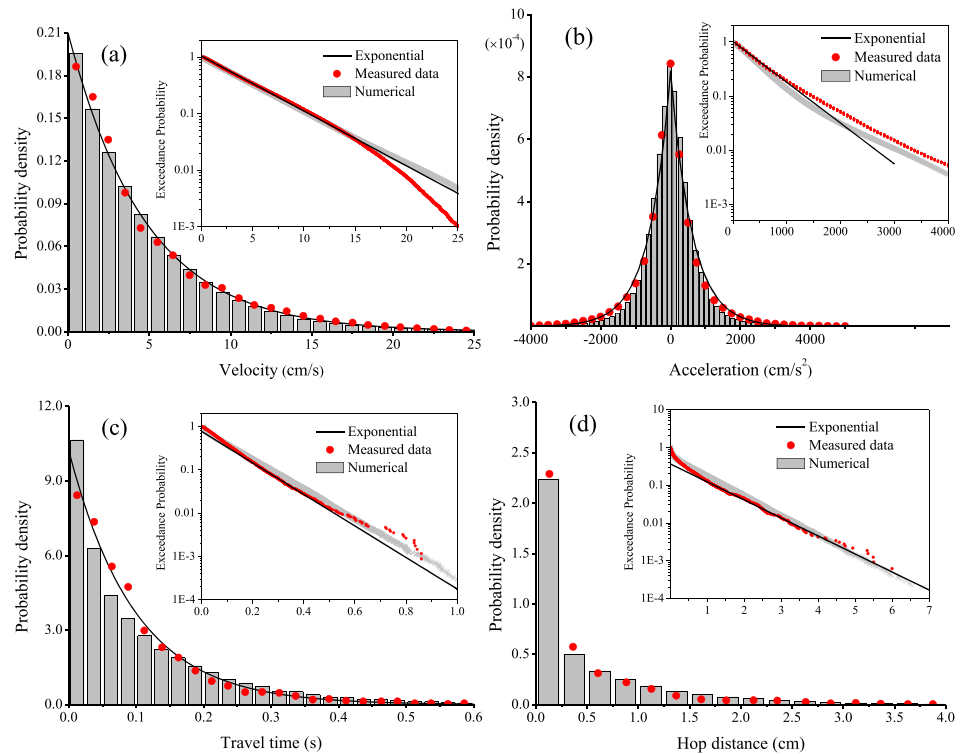


Figure 3. Comparison of numerically simulated and observed particle statistics. PDFs and exceedance probability distributions (insets) of particle (a) velocities, (b) accelerations, (c) travel times, and (d) hop distances from observations (red dots) and numerical simulation (vertical bars). The simulated particle motions are found entirely faithful to the experimental statistics. On all plots the fitted exponential distributions are shown only for comparison.

about 1 cm/s and an acceleration resolution of about 10^2 cm/s², and in part due to effects of deviations in the tail of the velocity distribution. Namely, the simulated particle velocity PDF is exponential (as specified by our numerical model; see equation (6)), slightly deviating from the observed exponential-like PDF in the tails (see Figure 2a inset). These small discrepancies do not affect the results, because further evidence demonstrating that our simulations faithfully mimic the experimental data is provided by comparing the simulated distributions of particle travel times (time in motion during a hop) T_p and hop distances L , which are shown to closely match the measured distributions (Figures 3c and 2d). It is noted that except for the measured mean of T_p , the travel times and hop distances were not used in fitting the numerical model. This physically informed numerical simulation is therefore shown to be faithful to the experimental statistics.

3.2. Transition in Scaling for Particle Hops

In previous studies a quadratic scaling ($L \sim T_p^2$) has been proposed (Fathel et al., 2015) for particle hop distances L and travel times T_p based on experimental data (see inset of Figure 4a). The apparent deviation from this scaling for large travel times/hop distances has been argued to be caused by experimental limitations (Fathel et al., 2015) and has thus been ignored. Namely, a possible censoring of large hop distances has been attributed to the limited size of the observed bed area (here 7.57 cm, the streamwise length of the cameral window).

A key finding of this work is that, whereas experimental censorship of motions (Ballio et al., 2019) may contribute to the appearance of such a scaling break, a regime transition in scaling from $L \sim T_p^2$ to $L \sim T_p$ for large hop distances is an inherent property of the dynamics of particle motion and is present even in the absence of any experimental limitation. This regime shift is clearly shown from our high-fidelity numerical simulation results, which do not suffer from any censoring, and it also becomes fully apparent with closer examination in the original experimental data (Figure 4a inset). To properly “unmask” and characterize the transition instead of merely inspecting the raw data, we filter the data by averaging hop distances within intervals of travel times of 0.004 s (Figure 4b). Remarkably, the experimental and simulated data yield virtually

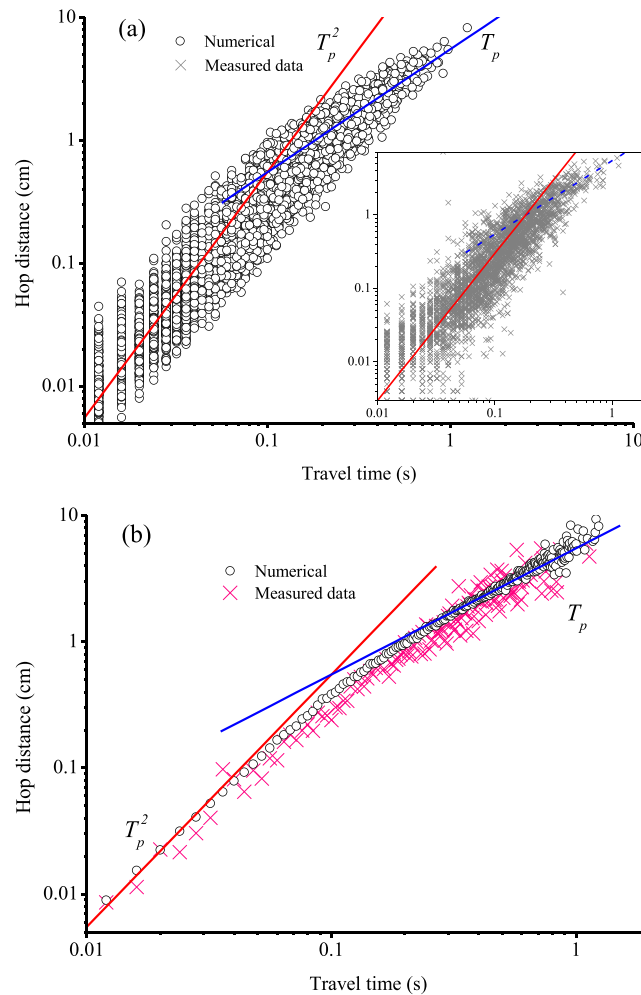


Figure 4. Two scaling regimes in hop distance/travel time. (a) Hop distance versus travel time as obtained from high-fidelity numerical simulations (main panel) and experimental data (inset figure); (b) overlapped plots of mean hop distance (averaged over intervals of 0.004 s) versus travel time for both numerical and experimental data. The existence of intrinsic differences between short- and long-hop particles is apparent suggesting two distinct scaling regimes. For this study, $T_p^* = 0.3$ s is estimated to demarcate the transition to long hop distance particles.

identical results in terms of a transition to a linear regime $L \sim T_p$ at long hop distances. We emphasize that this regime transition was not in any way hard coded in the numerical simulation (see also the last paragraph of the section 2.3). Specifically, the time scale of transition is found to be centered around 0.1 s, suggesting that travel times of $T_p \leq 0.07$ s and $T_p \geq 0.3$ s can be roughly adopted as thresholds identifying the two transport regimes of bedload particles regarded as “short” and “long” hops, respectively. The number of long-hop particles was respectively ~ 350 and $\sim 4,000$ for measured and simulated results, and the larger scatter starting from ~ 0.6 s in the simulated results is due to the limited number (~ 360) of particles that traveled longer than that time.

The transport regimes of short- and long-hop particles are quite different. Generally, only particles with long hop distances and with relatively long travel times (linear regime $L \sim T_p$) will have the chance to experience all (most) of the possible velocity states of the exponential-like PDF (Figure 3a). Thus, these particles will sample more frequently the tails of the PDF and on average achieve a higher mean velocity for the entire hop, thus approaching an almost constant value $\bar{u}_{pl} = L/T_p = \text{const}$, with angle brackets defining the average (see examples of simulated velocity sequences in Figure 5a and compare with the experimental plot in Figure 8 of reference by Roseberry et al., 2012). This is in contrast with the short-hop particles in the regime $L \sim T_p^2$, which have less of an opportunity to experience many velocity states in their short travel times. Moreover,

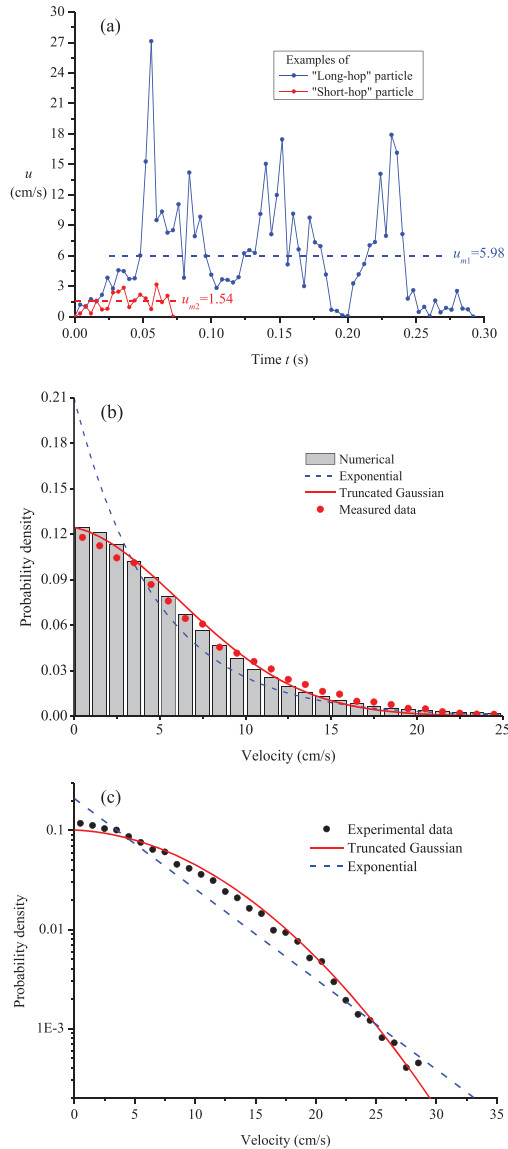


Figure 5. Comparison of the long- and short-hop particles. (a) Example of simulated velocity sequences of a typical short- and long-hop bedload particle, illustrating the fundamental differences in the two distinct regimes of particle motions. For long-hop particles, the mean velocity approaches a constant value (regime $L \sim T_p$). (b) The empirical velocity distribution of the long-hop particles for the experimental data (using $T_p \geq 0.35$ s) and numerical simulations (using $T_p \geq 0.5$ s), as well as the fitted truncated Gaussian velocity distribution. For comparison, the exponential-like distribution for all particles is shown. To calculate the PDFs, we first exclude particle hops from the data set with travel time T_p shorter than the chosen threshold, and then pool all the remaining velocities during every single hop for analysis. We demonstrate in Figure 6 that for long-hop particles ($L \sim T_p$), continuously increasing the threshold T_p^* has a negligible effect on the resulting velocity PDF, establishing thus the robustness of the adopted threshold of $T_p^* = 0.3$ s as defining the transition between long- and short-hop particle regimes. (c) The empirical velocity distribution of the long-hop particles for the experimental data shown in semilog plot, revealing differences in tails of the empirical and exponential distributions. A slightly adjusted parameter of $\tilde{\eta} = 0.116$ (instead of 0.14 for Figure 5b) is adopted for the truncated Gaussian distribution to better capture the tail of the empirical distribution.

due to the fact that short-hop particles must start and stop (both at zero velocity), these particles are expected to mostly finish the entire travel with relatively low velocities rendering their mean velocity proportional to their travel time, that is, $\bar{u}_{ps} = L/T_p \sim T_p$ (see Figure 7b in Furbish, Ball, & Schmeeckle, 2012). In other words, the large proportion of time the particle spent on starting (i.e., entrainment) and stopping (disentrainment) may be an important feature for short-hop particles (Campagnol et al., 2015). For particles of the same (or similar) size, it is thus interesting to examine effects of different flow conditions on bedload transport in terms of the two identified groups of particle motions, in which case Froude number can be seen as a reasonable measure of flow strength. Low-intensity subcritical flow involves far more short- than long-hop particles, whereas high-intensity supercritical flow involves proportionally more longer hops, the overall particle velocity statistics of which are expected to be different. We expect that under a higher flow strength, the particles are more likely to travel with higher velocity in general, and thus stay longer in motion. As a further step to take into account the effect of particle size, the Shields number may be used as an additional indicator describing the mobility of particles.

3.3. Unifying Observations of Different Velocity Distributions

Several research groups have recently reported measured instantaneous particle velocity distributions that can be described by distinct forms, respectively exponential (Furbish et al., 2016; Furbish & Schmeeckle, 2013; Heyman et al., 2016; Lajeunesse et al., 2010; Roseberry et al., 2012) and Gaussian like (Ancy & Heyman, 2014; Heyman et al., 2016; Martin et al., 2012). We note that particle motions (hop distances and travel times) for fixed bed (Martin et al., 2012) and mobile bed (Ancy & Heyman, 2014) experiments are not necessarily directly comparable; nonetheless, the velocities of moving particles show a Gaussian-like velocity PDF. While a probabilistic derivation has been proposed for the exponential-like distribution of bedload particle velocities (Furbish & Schmeeckle, 2013), the theoretical analysis of the Gaussian-like distribution was devised based on the mean-reverting (or Ornstein-Uhlenbeck) process (Ancy & Heyman, 2014), the Fokker-Planck equation representation of which is

$$\frac{\partial P}{\partial t} = \frac{\partial}{\partial u} \left(P \frac{u - u_s}{t_r} \right) + \frac{1}{t_r^2} \frac{\partial^2}{\partial u^2} (D_u P), \quad (11)$$

where $P(u, t)$ is the probability density function of the particle velocity u , t is the time, u_s is a constant average particle velocity, t_r is a relaxation time, and D_u is the equivalent of a particle diffusivity (constant). Under equilibrium transport conditions, the truncated Gaussian distribution (considering only positive particle velocities $u \geq 0$) as the solution of equation (11) can be derived:

$$P_{eq}(u \geq 0) = \sqrt{\frac{2}{\pi}} \frac{\eta}{1 + \operatorname{erf}\left(\frac{\eta}{\sqrt{2}} u_s\right)} \exp\left[-\eta^2 \frac{(u - u_s)^2}{2}\right], \quad (12)$$

where $\eta = \sqrt{t_r/D_u}$. Note that before truncation, u_s is the mode (most frequently occurring value) and also the mean of the Gaussian distribution. However, after truncation to the form of equation (12), generally u_s is no longer the mean but a parameter to be estimated by fitting the distribution to the data.

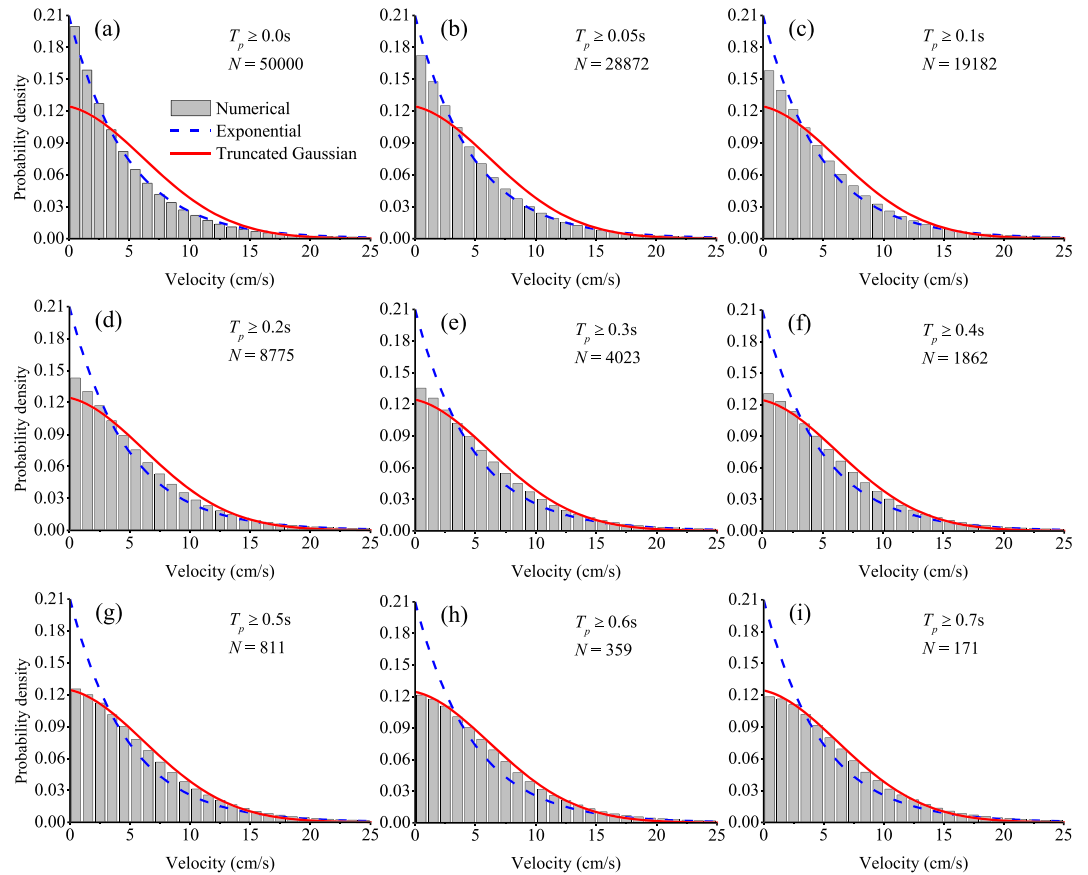


Figure 6. Transition from exponential- to truncated Gaussian-like velocity distribution for bedload particle hops. In each subfigure, particle hops with travel time T_p shorter than the threshold are removed from the data set of the 50,000 hops, and the remaining number of hops taken into consideration is N . We pooled all the velocity records during the N hops and calculated the velocity PDF. It is seen that in the linear scaling regime ($L \sim T_p^*$; empirically adopted for $T_p^* = 0.3$ s by Figure 4), continuously increasing the threshold T_p^* will have a negligible effect on the resulting velocity PDF. Due to the exponential distribution of travel times (Figure 3c), the particle number N taken into consideration in each subfigure drops rapidly as T_p^* increases. The exponential distribution (blue dash line) and the truncated Gaussian distribution (red solid line) in the subfigures are the same as those plotted in Figure 5b.

As also pointed out by Ancy and Heyman (2014), a crude approximation of the mean-reverting process (equation (11)) for the particle velocity U is given as

$$U(t) = u_m + \sqrt{2D_u} \cdot \xi(t), \quad (13)$$

where u_m represents the mean velocity and $\xi(t)$ is a white noise term. We note that equation (13) provides a fairly good description of the velocity fluctuations of our identified long-hop particles (the blue sequence in Figure 5a) around a properly defined constant mean. It is then theoretically expected that if we consider only the long-hop bedload particles (as a subset of the entire population of particles), the resulting velocity distribution will possess a Gaussian-like form.

To verify and further document this theoretical expectation, we analyzed bedload particles with travel time $T_p \geq 0.5$ s from the simulation results (obtaining 811 particle hop trajectories), and particles with $T_p \geq 0.35$ s from the experimental measurements. The probability distributions of particle velocities for the numerical and experimental results clearly demonstrate a truncated Gaussian form (with lower bound zero, considering only positive velocities), instead of an exponential (see Figure 5b). Recall that the threshold value of $T_p^* = 0.3$ s was identified as an empirical estimate that demarcates the transition from short- to long-hop particles (Figure 3b). We demonstrate in Figure 6 that once we are in the linear scaling

regime ($L \sim T_p$), continuously increasing the threshold T_p^* that defines the long-hop particles has a negligible effect on the resulting velocity PDF, providing evidence for the robustness of our results to the chosen value of $T_p^* = 0.3$ s.

Fitting the truncated Gaussian distribution equation (12) to the numerically simulated particle velocities gives the estimated parameters of $\hat{\eta} = 0.14$ and $\hat{u}_s = -1.0$ cm/s (Figure 5b). Note that equation (12) is a Gaussian distribution truncated at $u = 0$, that is, $P_{eq}(u \geq 0)$, and that in the above form the parameter u_s represents the mean and mode (the most frequently occurring value) of the Gaussian distribution before truncation. Thus, if the estimate of the parameter $\hat{u}_s \geq 0$, u_s continues to represent the mode of the truncated PDF. However, if the estimate $\hat{u}_s < 0$, u_s becomes just a fitting parameter and the mode is equal to zero. Compared with the positive estimate of \hat{u}_s (and therefore positive mode) obtained by Ancy and Heyman (2014), the negative estimate $\hat{u}_s = -1.0$ cm/s obtained herein (indicating thus a zero mode of the fitted truncated distribution; see also Figure 5b) implies that an insufficient proportion of particles traveled long enough to sample very large instantaneous velocities, thus preventing the appearance of a positive mode of $P(u)$. The direct relation of the form of the velocity PDF to the properties of the particle trajectories is worth noting and suggests that it could be explored to infer transport intensities from aggregate statistics.

4. Discussion

Recognizing and demonstrating the fundamental differences between particles that travel in short and long hops, we are able to provide a physical explanation for two different forms of the particle velocity distribution (exponential and Gaussian like, respectively) proposed in the literature, and connect the results with sediment and flow conditions during transport. It has been observed under subcritical flow conditions that particle motions with an exponential-like velocity distribution are dominated by short particle hops (Lajeunesse et al., 2010; Roseberry et al., 2012). In contrast, a Gaussian-like velocity distribution, which has been observed for supercritical flow conditions (Ancy & Heyman, 2014; Martin et al., 2012) is, according to our analysis, most likely to have been the result of long particle hops. This is consistent with observation for particles of similar size (or fixed mixture of sizes) that in supercritical flow with relatively strong flow strength (or high velocity), particles are more likely to move far from the bed and thus remain in motion longer as compared to subcritical flow (Heyman et al., 2016). However, in terms of grain mobility regarding different particle sizes, the Shields number may be an important indicator to consider in addition to the Froude number for comparing effects of different flow conditions on particle motions. Further efforts are needed to understand and characterize the conditions under which an exponential velocity distribution gives way to a Gaussian-like distribution. The ability to connect the different forms of the particle velocity distributions, physically and theoretically as done herein, to the particle trajectory characteristics can provide an important diagnostic tool to infer particle dynamics, and/or the flow conditions that modulate those dynamics. Grounding such diagnostic analysis on observed particle collective statistics has important practical implications and should be further pursued via targeted experimental and simulation studies.

Apart from the physically based explanation for the Gaussian-like particle velocity distribution as discussed herein (i.e., dominated by long-hop bedload particles), there is another less important but still possible cause for observing this distribution which is related to the choice of the sampling interval in experiments. Given that particle-tracking methods are still under development and that there is not yet consensus on protocols/expectations, in practice a frame rate that is up to an order of magnitude slower than 250 fps (the frame rate for data adopted in this paper) has been used (Martin et al., 2012). As the sampling interval increases, an increasing number of short-hop particles are not observed and the velocity distribution (computed from aggregate motions of the longer-hop particles) is bound to asymptotically approach a Gaussian, simply due to the Central Limit Theorem. Thus, our results provide a cautionary statement as to the interpretation of constrained experimental results relative to the underlying two-regime particle motions revealed herein.

Finally, since the form of the hop distance distribution is central to the entrainment form of the Exner equation and the calculation of sediment flux (Furbish, Haff, et al., 2012; Ganti et al., 2010; Parker et al., 2000), the two scaling regimes reported herein have significant theoretical and practical implications. Specifically, assuming an underlying exponential-like distribution of travel times (Fathel et al., 2015; Furbish et al., 2016;

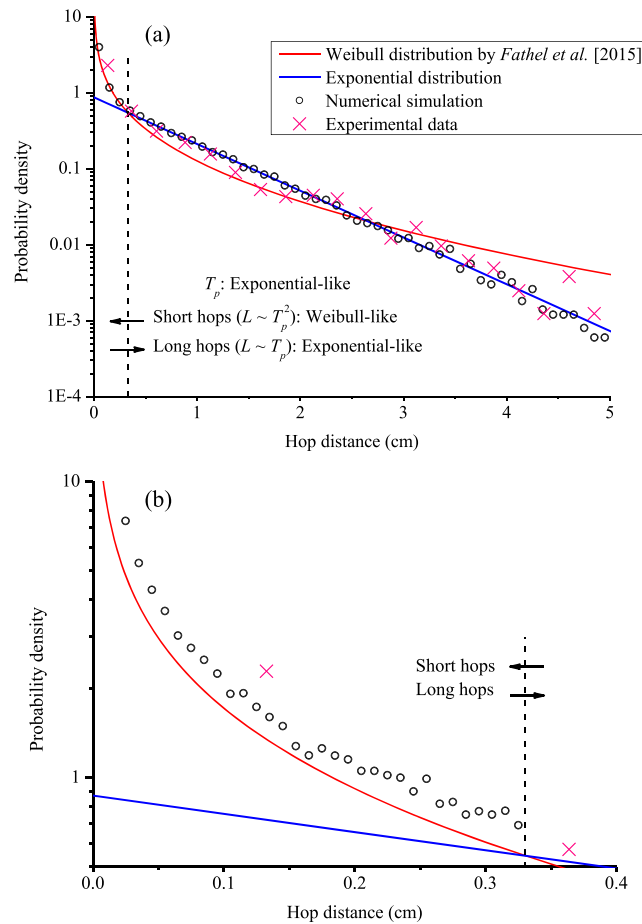


Figure 7. A mixed form of the hop distance distribution. (a) Assuming an underlying exponential-like distribution of travel times as reported in the literature (Fathel et al., 2015; Furbish et al., 2016; Martin et al., 2012), the two regimes for short- and long-hop particles identified in this paper give rise to a Weibull-like front and an exponential-like tail of the hop distance distribution. This represents strong evidence of a thin-tailed distribution of hop distances with important implications for bedload sediment transport formulations. (b) A detailed demonstration on the Weibull-like front of the distribution. We note that the Weibull distribution (red line) contains no fitted parameter, the form of which is adopted from equation (8) of Fathel et al. (2015): $f_L(L) = \frac{\sqrt{2/L}}{2L^{3/2}} \exp(-\sqrt{2/L} L^{1/2})$, with the measured mean hop distance $\langle L \rangle = 0.46$ cm.

Martin et al., 2012; Roseberry et al., 2012), the tail of the hop distance distribution is bound to be exponential-like in the linear scaling regime of $L \sim T_p$, while in the $L \sim T_p^2$ regime it is bound to be Weibull-like (see proof in Fathel et al. (2015)). Thus, our results suggest a mixed form (a Weibull-like front and an exponential-like tail) of the hop distance distribution (Figure 7), which should be incorporated in the probabilistic Exner equation. This result also represents strong evidence of a thin-tailed distribution for hop distances, which informs how we approach modeling of particle spreading, including the possibility of anomalous diffusion (Ganti et al., 2010; Schumer et al., 2009; Wu, Singh, et al., 2019).

We emphasize that the distribution of particle hop distances, together with the particle entrainment rate, are a centerpiece of entrainment formulations of the flux and the Exner equation (Furbish et al., 2017; Parker et al., 2000), and that these formulations are increasingly being examined and used to describe the sediment flux, bedform dynamics, and tracer particle behavior (Furbish et al., 2017; Ganti et al., 2010; Iwasaki et al., 2017). This represents a “return” to the pioneering work of Einstein (1937, 1950) and reflects that particle hop distances and entrainment are more closely related to the basic physics of particle motions than are the particle activity and velocities used in divergence formulations of the flux (Bridge & Dominic, 1984; Parker et al., 2003). This is particularly so in view of the growing recognition that the idea of an average

critical Shields stress, typically used in these formulations in geomorphic and engineering applications, is problematic (Dey & Ali, 2017; Masteller & Finnegan, 2017; Yager et al., 2015).

5. Conclusions

In this paper, we report an emergent regime shift in bedload particle motion characteristics (scaling laws and velocity statistics) under subcritical flow conditions (representing most natural flows) for particles that experience long travel times. Specifically, we show that particles whose motion is dominated by short hop distances follow a distance-time scaling regime of $L \sim T_p^2$, while particles which experience large hop distances transition to a different scaling regime of $L \sim T_p$. We provide a mechanistic explanation of this transition and show its presence in both experimental measurements (previously dismissed as censorship effects due to measurement limitation) and in numerical simulations, using a newly developed Lagrangian transport formulation of the Fokker-Planck equation.

We then argue that due to the linear scaling regime ($L \sim T_p$) of particles with long hop distances: (1) an exponential tail of travel times T_p is bound to produce an exponential tail of hop distances L as originally suggested by Einstein and recently reported by others and (2) due to the tendency to converge to an almost constant average particle velocity in that linear regime (the mean particle velocity $\bar{u}_{pl} = L/T_p = \text{const}$, with angle brackets defining the average), the fluctuations of instantaneous velocities of long-hop particles around that mean can be described by a Gaussian-like distribution, instead of the exponential-like distribution observed for all particles.

We highlight that depending on the flow conditions within which particle transport occurs, favoring the predominance of mostly short, mostly long, or a mixture of short and long hop distance particles, both the exponential-like and Gaussian-like particle velocity distributions can be observed. Thus, our observation of a regime transition in the probabilistic motion of particles and the hop distance/travel time scaling explains the disparate particle velocity distributions reported in the literature and puts them in a consistent theoretical setting within which interpretation of field and experimental observations can best be made.

Acknowledgments

The authors acknowledge support by the National Science Foundation (NSF) under Grant EAR-1209402 of the Water Sustainability and Climate (WSC) program, Grant EAR-1737872 under the project LIFE (Linked Institutions for Future Earth), and Grants EAR-1226076, EAR-1811909, and EAR-1735992. All the information for the theoretical analysis can be found in the text, and the data used are from published work, which has been properly referenced. We thank the Editor Ellen Wohl, the Associate Editor, Francesco Ballio, Mark Schmeeckle, and an anonymous reviewer for their constructive comments, which greatly improved this work.

References

- Ancey, C., & Heyman, J. (2014). A microstructural approach to bed load transport: Mean behaviour and fluctuations of particle transport rates. *Journal of Fluid Mechanics*, *744*, 129–168. <https://doi.org/10.1017/jfm.2014.74>
- Ballio, F., Radice, A., Fathel, S. L., & Furbish, D. J. (2019). Experimental Censorship of Bed Load Particle Motions, and Bias Correction of the Associated Frequency Distributions. *Journal of Geophysical Research: Earth Surface*, *124*, 116–136. <https://doi.org/10.1029/2018JF004710>
- Bridge, J., & Dominic, D. (1984). Bed load grain velocities and sediment transport rates. *Water Resources Research*, *20*(4), 476–490. <https://doi.org/10.1029/WR020i004p00476>
- Campagnol, J., Radice, A., Ballio, F., & Nikora, V. (2015). Particle motion and diffusion at weak bed load: Accounting for unsteadiness effects of entrainment and disentrainment. *Journal of Hydraulic Research*, *53*(5), 633–648. <https://doi.org/10.1080/00221686.2015.1085920>
- Dey, S., & Ali, S. Z. (2017). Stochastic mechanics of loose boundary particle transport in turbulent flow. *Physics of Fluids*, *29*(5), 77–102.
- Dimou, K. (1989). Simulation of estuary mixing using a two-dimensional random walk model, Massachusetts Institute of Technology.
- Dingle, E. H., Attal, M., & Sinclair, H. D. (2017). Abrasion-set limits on Himalayan gravel flux. *Nature*, *544*(7651), 471–474. <https://doi.org/10.1038/nature22039>
- Einstein, H. (1937). *Bedload transport as a probability problem. Sedimentation (reprinted in 1972)* (pp. 105–108). Colorado: Water Resources Publications.
- Einstein, H. A. (1950). The bed-load function for sediment transportation in open channel flows, US Department of Agriculture Washington, DC.
- Fan, N., Singh, A., Guala, M., Fofoula-Georgiou, E., & Wu, B. (2016). Exploring a semimechanistic episodic Langevin model for bed load transport: Emergence of normal and anomalous advection and diffusion regimes. *Water Resources Research*, *52*, 2789–2801. <https://doi.org/10.1002/2015WR018023>
- Fathel, S. L., Furbish, D. J., & Schmeeckle, M. W. (2015). Experimental evidence of statistical ensemble behavior in bed load sediment transport. *Journal of Geophysical Research: Earth Surface*, *120*, 2298–2317. <https://doi.org/10.1002/2015JF003552>
- Furbish, D., Fathel, S., & Schmeeckle, M. (2017). Particle motions and bed load theory: The entrainment forms of the flux and the Exner equation. In D. Tsutsumi & J. B. Laronne (Eds.), *Gravel-bed Rivers: Processes and Disasters* (pp. 97–120). Hoboken, NJ: John Wiley & Sons.
- Furbish, D. J., Ball, A. E., & Schmeeckle, M. W. (2012). A probabilistic description of the bed load sediment flux: 4. Fickian diffusion at low transport rates. *Journal of Geophysical Research*, *117*, F03034. <https://doi.org/10.1029/2012JF002356>
- Furbish, D. J., Haff, P. K., Roseberry, J. C., & Schmeeckle, M. W. (2012). A probabilistic description of the bed load sediment flux: 1. Theory. *Journal of Geophysical Research*, *117*, F03031. <https://doi.org/10.1029/2012JF002352>
- Furbish, D. J., Roseberry, J. C., & Schmeeckle, M. W. (2012). A probabilistic description of the bed load sediment flux: 3. The particle velocity distribution and the diffusive flux. *Journal of Geophysical Research*, *117*, F03033. <https://doi.org/10.1029/2012JF002355>
- Furbish, D. J., & Schmeeckle, M. W. (2013). A probabilistic derivation of the exponential-like distribution of bed load particle velocities. *Water Resources Research*, *49*, 1537–1551. <https://doi.org/10.1002/wrcr.20074>

- Furbish, D. J., Schmeeckle, M. W., Schumer, R., & Fathel, S. L. (2016). Probability distributions of bed load particle velocities, accelerations, hop distances, and travel times informed by Jaynes's principle of maximum entropy. *Journal of Geophysical Research: Earth Surface*, *121*, 1373–1390. <https://doi.org/10.1002/2016JF003833>
- Ganti, V., Meerschaert, M. M., Foufoula-Georgiou, E., Viparelli, E., & Parker, G. (2010). Normal and anomalous diffusion of gravel tracer particles in rivers. *Journal of Geophysical Research*, *115*, F00A12. <https://doi.org/10.1029/2008JF001222>
- Hassan, M. A., Voepel, H., Schumer, R., Parker, G., & Fraccarollo, L. (2013). Displacement characteristics of coarse fluvial bed sediment. *Journal of Geophysical Research: Earth Surface*, *118*, 155–165. <https://doi.org/10.1029/2012JF002374>
- Heyman, J., Bohorquez, P., & Ancey, C. (2016). Entrainment, motion, and deposition of coarse particles transported by water over a sloping mobile bed. *Journal of Geophysical Research: Earth Surface*, *121*, 1931–1952. <https://doi.org/10.1002/2015JF003672>
- Hill, K. M., DellAngelo, L., & Meerschaert, M. M. (2010). Heavy-tailed travel distance in gravel bed transport: An exploratory enquiry. *Journal of Geophysical Research*, *115*, F00A14. <https://doi.org/10.1029/2009JF001276>
- Hoefel, F., & Elgar, S. (2003). Wave-induced sediment transport and sandbar migration. *Science*, *299*(5614), 1885–1887. <https://doi.org/10.1126/science.1081448>
- Hosseini-Sadabadi, S. A., Radice, A., & Ballio, F. (2019). On reasons of the scatter of literature data for bed-load particle hops. *Water Resources Research*, *55*, 1698–1706. <https://doi.org/10.1029/2018WR023350>
- Houssais, M., Ortiz, C. P., Durian, D. J., & Jerolmack, D. J. (2015). Onset of sediment transport is a continuous transition driven by fluid shear and granular creep. *Nature Communications*, *6*(1), 6527. <https://doi.org/10.1038/ncomms7527>
- Iwasaki, T., Nelson, J., Shimizu, Y., & Parker, G. (2017). Numerical simulation of large-scale bed load particle tracer advection-dispersion in rivers with free bars. *Journal of Geophysical Research: Earth Surface*, *122*, 847–874. <https://doi.org/10.1002/2016JF003951>
- Kidanemariam, A. G., & Uhlmann, M. (2014). Direct numerical simulation of pattern formation in subaqueous sediment. *Journal of Fluid Mechanics*, *750*. <https://doi.org/10.1017/jfm.2014.284>
- Lajeunesse, E., Malverti, L., & Charru, F. (2010). Bed load transport in turbulent flow at the grain scale: Experiments and modeling. *Journal of Geophysical Research*, *115*, F04001. <https://doi.org/10.1029/2009JF001628>
- Lançon, P., Batrouni, G., Lobry, L., & Ostrowsky, N. (2001). Drift without flux: Brownian walker with a space-dependent diffusion coefficient. *EPL (Europhysics Letters)*, *54*(1), 28–34. <https://doi.org/10.1209/epl/i2001-00103-6>
- Martin, R. L., Jerolmack, D. J., & Schumer, R. (2012). The physical basis for anomalous diffusion in bed load transport. *Journal of Geophysical Research*, *117*, F01018. <https://doi.org/10.1029/2011JF002075>
- Masteller, C. C., & Finnegan, N. J. (2017). Interplay between grain protrusion and sediment entrainment in an experimental flume. *Journal of Geophysical Research: Earth Surface*, *122*, 274–289. <https://doi.org/10.1002/2016JF003943>
- Nikora, V., Habersack, H., Huber, T., & McEwan, I. (2002). On bed particle diffusion in gravel bed flows under weak bed load transport. *Water Resources Research*, *38*(6), 1081. <https://doi.org/10.1029/2001WR000513>
- Parker, G., Paola, C., & Leclair, S. (2000). Probabilistic Exner sediment continuity equation for mixtures with no active layer. *Journal of Hydraulic Engineering*, *126*(11), 818–826. [https://doi.org/10.1061/\(ASCE\)0733-9429\(2000\)126:11\(818\)](https://doi.org/10.1061/(ASCE)0733-9429(2000)126:11(818))
- Parker, G., Seminara, G., & Solari, L. (2003). Bed load at low Shields stress on arbitrarily sloping beds: Alternative entrainment formulation. *Water Resources Research*, *39*(7), 1183. <https://doi.org/10.1029/2001WR001253>
- Roseberry, J. C., Schmeeckle, M. W., & Furbish, D. J. (2012). A probabilistic description of the bed load sediment flux: 2. Particle activity and motions. *Journal of Geophysical Research*, *117*, F03032. <https://doi.org/10.1029/2012JF002353>
- Schmeeckle, M. W. (2014). Numerical simulation of turbulence and sediment transport of medium sand. *Journal of Geophysical Research: Earth Surface*, *119*, 1240–1262. <https://doi.org/10.1002/2013JF002911>
- Schumer, R., Meerschaert, M. M., & Baeumer, B. (2009). Fractional advection-dispersion equations for modeling transport at the Earth surface. *Journal of Geophysical Research*, *114*, F00A07. <https://doi.org/10.1029/2008JF001246>
- Voller, V. R., & Paola, C. (2010). Can anomalous diffusion describe depositional fluvial profiles? *Journal of Geophysical Research*, *115*, F00A13. <https://doi.org/10.1029/2009JF001278>
- Wilcock, P. R. (1998). Two-fraction model of initial sediment motion in gravel-bed rivers. *Science*, *280*(5362), 410–412. <https://doi.org/10.1126/science.280.5362.410>
- Wong, M., Parker, G., DeVries, P., Brown, T. M., & Burges, S. J. (2007). Experiments on dispersion of tracer stones under lower-regime plane-bed equilibrium bed load transport. *Water Resources Research*, *43*, W034403. <https://doi.org/10.1029/2006WR005172>
- Wu, Z., Foufoula-Georgiou, E., Parker, G., Singh, A., Fu, X., & Wang, G. (2019). Analytical solution for anomalous diffusion of bedload tracers gradually undergoing burial. *Journal of Geophysical Research: Earth Surface*, *124*, 21–37. <https://doi.org/10.1029/2018JF004654>
- Wu, Z., Singh, A., Fu, X., & Wang, G. (2019). Transient anomalous diffusion and advective slowdown of bedload tracers by particle burial and exhumation. *Water Resources Research*, *55*, 7964–7982. <https://doi.org/10.1029/2019WR025527>
- Yager, E., Kenworthy, M., & Monsalve, A. (2015). Taking the river inside: Fundamental advances from laboratory experiments in measuring and understanding bedload transport processes. *Geomorphology*, *244*, 21–32. <https://doi.org/10.1016/j.geomorph.2015.04.002>